Optica Applicata, Vol. LII, No. 3, 2022
DOI: 10.37190/oa220309

Spectral analysis for tilted fiber Bragg gratings in the corrosion detection for concrete structure

Kok Zee Kwong[1], Waldo Udos[2], Kok-Sing Lim[2*], Foo Wei Lee[1], Chee Ghuan Tan[3], Muhamad Zharif Samion[2], Harith Ahmad[2]

[1]Civil Engineer Department, Universiti Tunku Abdul Rahman, Sungai Long Campus, Bandar Sungai Long, Cheras 43000, Kajang, Selangor, Malaysia

[2]Photonics Research Centre, Universiti Malaya, 50603 Kuala Lumpur, Malaysia

[3]Department of Civil Engineering, Faculty of Engineering, Universiti Malaya, 50603 Kuala Lumpur, Malaysia

[*]Corresponding author: kslim@um.edu.my

An effective corrosion monitoring technique is sought after by the engineers for assessing the steel bar corrosion at the early stage for the maintenance and repair works, especially in the corrosive environments, such as coastal and marine. In this work, tilted fiber Bragg grating (TFBG) with the optical sensor is employed in corrosion monitoring of a reinforced concrete structure. Taking advantage of the high sensitivity of TFBG cladding resonance wavelengths to the change in the surrounding medium, the sensor is mounted on the steel bar that is embedded in a concreted block during an accelerated corrosion process. The acquired transmission spectrum of the TFBG during the procedure is digitally processed using Fourier Transform to produce an index that is sensitive to the generated corrosion product surrounding the TFBG sensor. This eases the analysis of the sophisticated TFBG transmission spectra. The generated index can be used as an indicator (indicator J) for the corrosion process of the embedded steel bar in the concrete structure. This indicator J can act as an indicator to describe the corrosion activity and corrosion level at a specific point of the steel bar in concrete structures.

Keywords: tilted fiber Bragg grating, optical spectral analysis, Fourier transform, corrosion, steel bar.

1. Introduction

Reinforced concrete has been widely used in engineering structures, namely the water dams, jetties, harbours and bridges in many marine environments. However, compared to inland locations, the corrosive environment of coastal and marine has increased the risk of corrosive damages to the steel reinforcement inside the concrete structure, resulting in the loss of steel area, cracking and spalling of the concrete. Hence, an effective corrosion monitoring technique is sought after by the engineers for assessing the steel bar corrosion at the early stage for the maintenance and repair works.

The corrosion condition of the steel reinforcement of the concrete structure is desired to be examined periodically from the beginning of the construction phase. The corrosion rate of steel reinforcement can be measured by using the market available non-destructive testing techniques. However, these techniques are limited to corrosion rate estimation without interpreting the corrosion level in wet conditions [1].

Corrosion measurement and monitoring is a complicated process involving several considerations and strategies in implementation. Open circuit potential (OCP) measurement is one of the typical measurements of steel reinforcement corrosion concerning the $Cu/CuSO_4$ electrode (CSE), Ag/AgCl electrode and saturated calomel electrode (SCE) in accordance with ASTM C 876 Standard Test Method for Half-Cell Potential of Reinforcing Steel in Concrete [2]. It indicates the potential developed by the metal when it reacts with the environment. Hence, OCP monitoring measurement has become the most common technique for the periodic inspection of the reinforced concrete structures [3-5].

While, in terms of detecting steel reinforcement corrosion, half-cell potential (HCP) measurement is the most common non-destructive testing technique. In the reinforced concrete structures, depending on the environment, the concrete that acts as an electrolyte will lead the development of potential by the steel reinforcement. Therefore, this measurement will provide data on the corrosion rate of the steel reinforcement inside the reinforced concrete structures. Other techniques in measuring corrosion level include the polarization resistance technique, which is based on the chloride threshold [6], cement seawater battery energy harvester technique [7] and electrochemical techniques [8].

There are few methods to collect the data for the corrosion measurement and monitoring, including the installation of an embedded corrosion monitoring sensor (ECMS) [9, 10], vibrating wire, electrical strain gauges and optical fibre sensors (OFS) [11]. A corrosion process in steel reinforcement involves the electrochemical transformations which can be detected by OFS. The corrosion rate varies at a different location along the steel reinforcement as the nature of corrosion is localized. Recent development proposed that an advanced OFS has the capability to be applied for multiple functions. This makes the OFS a cost-effective system that can be applied to collect data even from few sensors in a different location of the concrete structures.

OFS has proved effective in the non-destructive evaluation (NDE) for bridge piers, buildings, water dams, flood control channels and erosion control structures. OFS collects and delivers all the data without demanding the *in situ* core samples from the structures, which will cause damages to the structures. OFS is a small and compact sensor that has advantages in remote sensing and continuous monitoring capability [12, 13]. Recently, the application of OFS for structural health monitoring (SHM) of concrete structures has become an intense study for corrosion monitoring and micro-cracks detection in concrete [14-21]. These studies include the research conducted by employing fiber Bragg gratings sensors (FBGS) [15-16, 19, 22-23], long-period gratings (LPGs) [24], interferometer-based optical sensors [17-18, 20], intensity-based optical sensors [14, 21], metal cladding optical fiber [25-26], point optical fiber sensor [27], twin-fiber technique [17] and plastic optical fibers [21]. These studies have laid a foundation on the

technical assessment and demonstrate the potential of OFS technology for the SHM of concrete structures.

In the recent year, tilted fiber Bragg grating (TFBG) has been targeted in numerous industrial sensing applications, including magnetic field sensing [28], temperature-independent vibration measurement [29], twist/torsion measurement [30], strain measurement [31] and concentration sensor [32]. The inscription of tilted grating in the single-mode fiber will contribute to the excitation of cladding modes in the fiber [33]. The core-cladding mode couplings lead to the generation of multiple cladding resonance wavelengths in the transmission spectrum. Since the cladding modes have more robust interaction with the surrounding medium, the cladding resonance wavelengths can be used as sensing parameters for the surrounding refractive index (SRI) [34-36].

MAGUIS *et al*. [37] proposed the use of the Fourier Transformation that converts the complex transmission spectra into a simplified form. The peak frequency linearly shifts with increasing SRI. The analysis can be applied with the FBGS in corrosion detection in the reinforced concrete structures. The corrosion of the steel reinforcement was accelerated in this research by applying the impressed current technique. The corrosion rate was monitored based on the results of changes in the transmission spectrum. The application of a TFBG sensor for steel reinforcement corrosion monitoring using the Fourier Transformation signal processing technique is presented.

2. Theories of accelerated corrosion

The steel reinforcement corrosion condition can be measured from the mass loss during the corrosion process. According to IJSSELING [38], the steel rust produced from the steel reinforcement (per unit surface area) can be estimated by applying Faraday's law based on the time period and applied current, as presented in the following equation:

$$\Delta W = MIt/ZF$$

where ΔW is the mass loss for steel reinforcement (g), I is the current (A), t is the time (s), F is 96 487 C/mol (Faraday's constant), Z is the number of the transferred electrons for Fe(2), and M is 55.847 g/mol for steel (molar mass).

In the experiment, the current-impressed technique was applied to accelerate the corrosion rate of the steel reinforcement at a constant current I of 80 mA for about 2 days (2880 min). Faraday's law was then used to determine the theoretical amount of induced corrosion based on the time period and applied current.

3. Material and experimental setup

In this study, three concrete samples of size 120 mm (length) × 120 mm (width) × 60 mm (height) were prepared according to the concrete composition presented in the Table. The cement used for the sample was Type 1 ordinary Portland cement (OPC) from Tasek Corporation Berhad, Malaysia, for the general concrete application with quality conforms to EN 196. The quarry aggregates with the size ranging from 4.75 to 20 mm and

T a b l e. Concrete composition for the samples.

Material	Weight [kg]
Cement	0.60
Water	0.32
Coarse aggregate (from 4.75 to 20 mm)	1.18
Fine aggregate	1.19

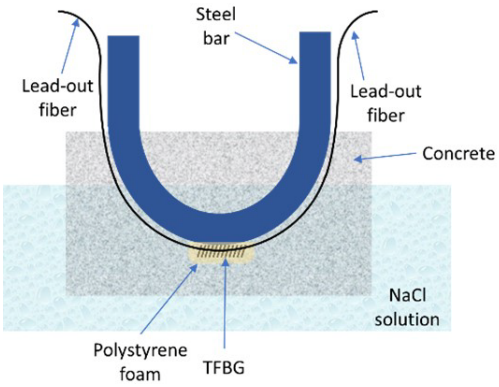

Fig. 1. Sample setup.

river sand were used as the coarse and fine aggregate in the concrete samples. A 10 mm diameter U-shaped steel reinforcement of 440 mm length (comply to MS146:2006 with Grade 500) from Southern Steel Group was embedded in the concrete block. The TFBG sensor was mounted on the bottom surface of the steel reinforcement, as illustrated in Fig. 1. The distance between the TFBG sensor and the bottom surface of the concrete is 20 mm. A small piece of polystyrene foam of size 20 mm (length) × 10 mm (width) × 10 mm (height) was used as the buffer to isolate and protect TFBG from the concrete mixture during the casting process. The samples were soaked in sodium chloride (NaCl) solution.

The current-impressed technique was applied to induce corrosion for the steel reinforcement. It was conducted by applying a direct-current (DC) power source using an electrolyte and a counter electrode. One steel reinforcement embedded in concrete block acts as the anode, whereas another similar steel reinforcement serves as the cathode in the electric circuit. The distance between the cathode and anode steel reinforcements was 180 mm. Both steel reinforcements were immersed in the NaCl solution (190 g of NaCl salt in 12.5 L of water). A constant electric current of 80 mA was supplied to the steel bar throughout the experiment to accelerate the corrosion process. However, the resistance of the circuit was increased with time, and the current slowly decayed to 50 mA.

The TFBG sensor was attached at the bottom surface of the steel reinforcement, which connected to the anode electrically. The TFBG used in this experiment was 15 mm in length with the Bragg wavelength of 1563.6 nm. The experiment was con-

ducted in a laboratory with air-conditioning, where the room temperature was maintained to be 24 °C (±1 °C) in order to provide a consistent environment for corrosion cell formation. The transmission spectra were analyzed by using an optical spectrum analyzer (AQ6317B, ANDO) and recorded by the LabVIEW program on a laptop via a GBIP-USB card. The amplified spontaneous emission of an erbium-doped fiber amplifier in the range of 1500–1570 nm was used as an optical broadband source for illuminating the TFBG. The data recording was conducted every 30 minutes for a total duration of 2880 minutes (48 hours) in the corrosion process that was accelerated by the current-impressed technique. A schematic diagram description for the spectral analysis and signal processing will be presented in the next section.

4. Results and discussion

Figure 2 shows the bottom view of the concrete sample. The sample was then hacked into half with the exposure of the steel bar (Figs. 3 and 4). The embedded steel bar was

Fig. 2. Bottom view of the concrete sample.

Fig. 3. The concrete sample was hacked with exposure of the steel bar.

Fig. 4. The rusts on the steel bars.

removed from the concrete and cleaned before the weight measurement. It is found that the steel bar lost 3.2 g of mass (2.15%) after 48 hours of accelerated corrosion.

Figure 5**a** shows the evolution of the TFBG transmission spectrum during the current-impressed corrosion process at an initial electric current of 80 mA over a duration of 2880 minutes (48 hours). Most of the cladding mode resonances are subject to a similar reduction in amplitude. It was believed that the creation of insoluble corrosion products such as Fe_3O_4 and FeOOH [33] settled in the proximity with the fiber glass surface, and they were opaque substances that could induce optical scattering and attenuation to the evanescent wave and intensities of the cladding modes in the TFBG. That led to the increasing loss to all the cladding modes in the fiber glass. This explains the decrease in amplitudes of cladding mode resonances in the transmission spectrum during the corrosion progress. Figure 5**b** shows the temperature-compensated wavelength shifts ($\Delta\lambda_c - \Delta\lambda_B$) of three different cladding resonances at 1518.2, 1528.4 and

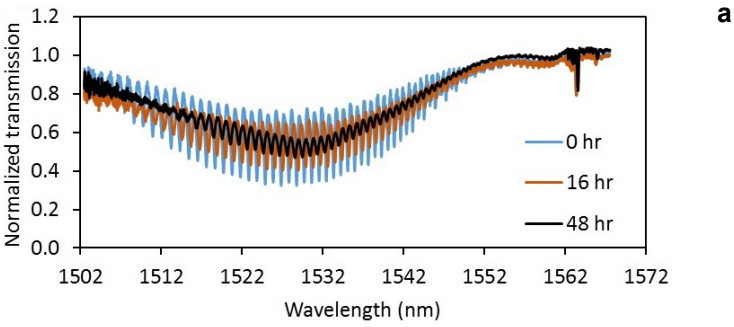

Fig. 5. (**a**) Evolution of the TFBG transmission spectrum. (**b**) Wavelength shifts of the cladding resonances at 1518.2, 1528.4 and 1538 nm. (**c**) Sensitivity to the corrosion (nm/%) for some of the cladding resonances during the current-impressed corrosion process for 2880 min (48 hours).

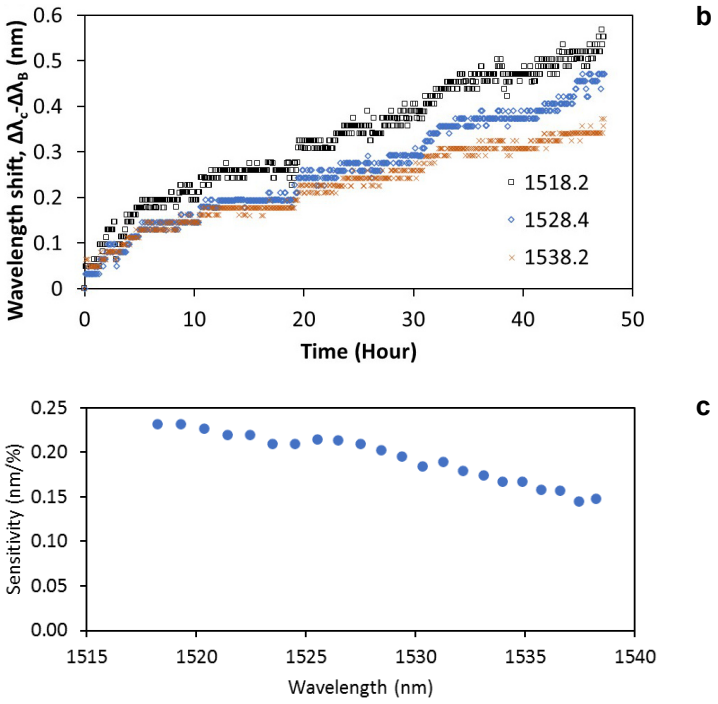

Fig. 5. Continued.

1538 nm during the corrossion process. The notation $\Delta\lambda_c$ represents the wavelength shift of the cladding resonance whereas $\Delta\lambda_B$ represents the wavelength shift of the Bragg wavelength at ~1563.6 nm. The red-shifts of the cladding resonances ($\Delta\lambda_c - \Delta\lambda_B$) can be attributed to the increasing refractive index (RI) of the saline solution during the corrosion process. The sensitivities of the cladding resonances are found to be in the order of 1518.2 nm > 1528.4 nm > 1538.2 nm. This is because the cladding resonances in the shorter wavelength are associated with the higher order cladding modes that have stronger evanescent field at the cladding-ambient medium interface and higher RI sensitivity to the ambient medium. Figure 5**c** shows the corrosion sensitivities of some of the cladding resonances to corrosion. The corrosion sensitivities are calculated based on the calculated average corrosion rate of 0.04%/h. In our previous work [39] we stated that the wavelength shifts of the cladding resonances can serve as indicators for the corrosion process. However, this method suffers from some shortcomings, for instance the fact that the complex transmission spectrum contains many cladding resonances and the different RI sensitivity for every cladding resonance. An accurate identification of the cladding resonance and correctct mapping of the corresponding sensitivity are required for demodulating the spectrum of the TFBG sensor. Furthermore, the diminishing amplitudes of the cladding resonances during the corrosion process make the detection of wavelength shifts very challenging and the results can be erroneous when the amplitudes are small at the later stage of the corrosion process.

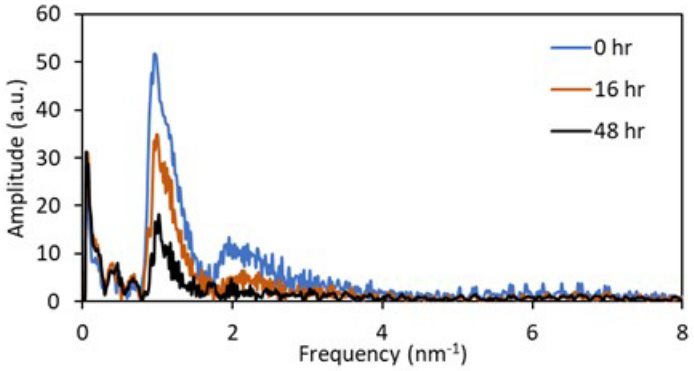

Fig. 6. The Fourier transforms of the transmission spectra as shown in Fig. 5.

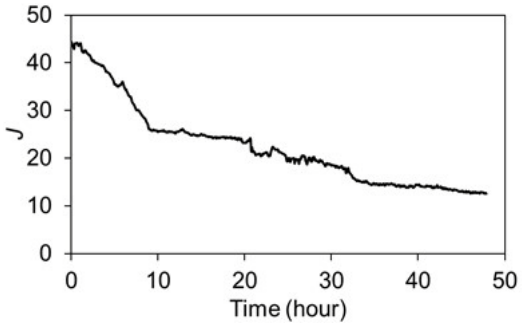

Fig. 7. Variation of indicator J with time during the current-impressed corrosion process.

Following that, Fourier transform [37] was applied to convert the transmission spectra into spatial frequency spectra as shown in Fig. 6. The conversion was performed using the fast Fourier transform, FFT(·) function in MATLAB. Before the conversion, the DC block filter was first applied to the transmission spectrum by subtracting its mean value and eliminating the large amplitude component at the 0 nm^{-1} in the frequency spectrum. The signal in the frequency range of 0.8 to 8 nm^{-1} was responsive to the corrosion process and its diminishing characteristic was consistent with the decreasing amplitude of the cladding resonances in Fig. 3. On the other hand, the signal in the range of 0.0 to 0.8 nm^{-1} remains almost the same throughout the corrosion process. Let J be the integral of signal curve from 0.8 to 8 nm^{-1} in the frequency spectrum (see Fig. 6). It is found that J decreases almost monotonically during the corrosion process, as depicted in Fig. 7. Based on the measured total mass loss, ΔM of 3.2 g or 2.15%, the average electric current is estimated to be around 64 mA. The average corrosion rate over 48 hours of accelerated corrosion is around 0.04%/h. Therefore, the parameter J can be used as the indicator for the corrosion monitoring and on-site measurement for the steel reinforcement in concrete structures. Moreover, it can be used to describe the corrosion activity at a specific point of the steel bar in concrete

structures. The compact size of the TFBG makes it a minimum invasive sensor suitable for embedment in the concrete structure without compromising its structural integrity.

5. Conclusion

The study has presented the application of TFBG sensor in the monitoring of the steel bars in a concrete structure immersed in NaCl solution. The steel reinforcement corrosion process was accelerated by applying the Current-impressed technique. Fourier transform analysis was used to convert the transmission spectra into frequency spectra. During the corrosion process, it was observed that the amplitude of the cladding resonances deceased along with time. The decreasing amplitude of the cladding resonances can be used for the on-site measurement and monitoring of steel reinforcement corrosion conditions in marine concrete structures. Moreover, the indicator J presented in the study is a single-value indicator that describes the corrosion activity at a specific point of the steel bar in concrete structures. The calibration relationship between the J indicator and the corrosion condition of the steel reinforcement should be established further before the application in real-life corrosion monitoring.

Acknowledgements
The work is supported by the Impact-Oriented Interdisciplinary Research Grant, Universiti Malaya, (IIRG028A-2019).

References

[1] Sørensen H.E., Frølund T., *Monitoring of reinforcement corrosion in marine concrete structures by the galvanostatic pulse method*, [In] *Proceedings of International Conference on Concrete in Marine Environments*, Hanoi-Vietnam, 2002.
[2] ASTM C876-91 R99. Standard Test Method for Half-Cell Potentials of Uncoated Reinforcing-Steel in Concrete. West Conshohocken, PA: ASTM, 2005.
[3] Aguirre-Guerrero A.M., Robayo-Salazar R.A., de Gutiérrez R.M., *A novel geopolymer application: Coatings to protect reinforced concrete against corrosion*, Applied Clay Science **135**, 2017, pp. 437–446, DOI: 10.1016/j.clay.2016.10.029.
[4] Subbiah K., Velu S., Kwon S.J., Lee H.S., Rethinam N., Park D.J., *A novel in-situ corrosion monitoring electrode for reinforced concrete structures*, Electrochimica Acta **259**, 2018, pp. 1129–1144, DOI: 10.1016/j.electacta.2017.10.088.
[5] Wang F., Xu J., Xu Y., Jiang L., Ma G., *A comparative investigation on cathodic protections of three sacrificial anodes on chloride-contaminated reinforced concrete*, Construction and Building Materials **246**, 2020, 118476, DOI: 10.1016/j.conbuildmat.2020.118476.
[6] Wu Z., Yu H., Ma H., Zhang J., Da B., Zhu H., *Rebar corrosion in coral aggregate concrete: Determination of chloride threshold by LPR*, Corrosion Science **163**, 2020, 108238, DOI: 10.1016/j.corsci.2019.108238.
[7] Ouellette S.A., Todd M.D., *Cement seawater battery energy harvester for marine infrastructure monitoring*, IEEE Sensors Journal **14**(3), 2014, pp. 865–872, DOI: 10.1109/JSEN.2013.2290492.
[8] Wu Z., Yu H., Ma H., Da B., Tan Y., *Rebar corrosion behavior of coral aggregate seawater concrete by electrochemical techniques*, Anti-Corrosion Methods and Materials **67**(1), 2020, pp. 59–72, DOI: 10.1108/ACMM-05-2019-2128.

[9] LIU P., HU Y., GENG B., XU D., *Corrosion monitoring of the reinforced concrete by using the embedded annular piezoelectric transducer*, Journal of Materials Research and Technology **9**(3), 2020, pp. 3511–3519, DOI: 10.1016/j.jmrt.2020.01.088.

[10] RAMÓN J.E., MARTÍNEZ I., GANDÍA-ROMERO J.M., SOTO J., *An embedded-sensor approach for concrete resistivity measurement in on-site corrosion monitoring: Cell constants determination*, Sensors **21**(7), 2021, 2481, DOI: 10.3390/s21072481.

[11] SING D.V., SACHA A.K., RAWA A., *Developments in corrosion detection techniques for reinforced concrete structures*, Indian Journal of Science and Technology **9**(30), 2016, pp. 1–6, DOI: 10.17485/ijst/2016/v9i30/99205.

[12] BREMER K., WEIGAND F., ZHENG Y., ALWIS L.S., HELBIG R., ROTH B., *Structural health monitoring using textile reinforcement structures with integrated optical fiber sensors*, Sensors **17**(2), 2017, 345, DOI: 10.3390/s17020345.

[13] MAO J., CHEN J., CUI L., JIN W., XU C., HE Y., *Monitoring the corrosion process of reinforced concrete using BOTDA and FBG sensors*, Sensors **15**(4), 2015, pp. 8866–8883, DOI: 10.3390/s150408866.

[14] ROSSI P., LE MAOU F., *New method for detecting cracks in concrete using fibre optics*, Materials and Structures **22**(6), 1989, pp. 437–442, DOI: 10.1007/BF02472221.

[15] DAVIS M.A., BELLEMORE D.G., KERSEY A.D., *Distributed fiber Bragg grating strain sensing in reinforced concrete structural components*, Cement and Concrete Composites **19**(1), 1997, pp. 45–57, DOI: 10.1016/S0958-9465(96)00042-X.

[16] MAASKANT R., ALAVIE T., MEASURES R.M., TADROS G., RIZKALLA S.H., GUHA-THAKURTA A., *Fiber -optic Bragg grating sensors for bridge monitoring*, Cement and Concrete Composites **19**(1), 1997, pp. 21–33, DOI: 10.1016/S0958-9465(96)00040-6.

[17] PNG W.H., LIN H.S., PUA C.H., LIM J.H., LIM S.K., LEE Y.L., RAHMAN F.A., *Feasibility use of in-line Mach–Zehnder interferometer optical fibre sensor in lightweight foamed concrete structural beam on curvature sensing and crack monitoring*, Structural Health Monitoring **17**(5), 2018, pp. 1277–1288, DOI: 10.1177/1475921718792108.

[18] WEI H., LIAO K., ZHAO X., KONG X., ZHANG P., SUN C., *Low-coherent fiber-optic interferometry for in situ monitoring the corrosion-induced expansion of pre-stressed concrete cylinder pipes*, Structural Health Monitoring **18**(5–6), 2019, pp. 1862–1873, DOI: 10.1177/1475921719826360.

[19] DENG F., HUANG Y., AZARMI F., *Corrosion detection for steel with soft coating using in-line fiber Bragg grating sensor*, Proc. SPIE 10168, Sensors and Smart Structures Technologies for Civil, Mechanical, and Aerospace Systems 2017, 101681R, DOI: 10.1117/12.2260260.

[20] BONFIGLIOLI B., PASCALE G., *Internal strain measurements in concrete elements by fiber optic sensors*, Journal of Materials in Civil Engineering **15**(2), 2003, pp. 125–133, DOI: 10.1061/(ASCE)0899-1561(2003)15:2(125).

[21] KUANG K.S.C., AKMALUDDIN, CANTWELL W.J., THOMAS C., *Crack detection and vertical deflection monitoring in concrete beams using plastic optical fibre sensors*, Measurement Science and Technology **14**(2), 2003, pp. 205–216, DOI: 10.1088/0957-0233/14/2/308.

[22] MAO J., XU F., GAO Q., LIU S., JIN W., XU Y., *A monitoring method based on FBG for concrete corrosion cracking*, Sensors **16**(7), 2016, 1093, DOI: 10.3390/s16071093.

[23] ALMUBAIED O., CHAI H.K., ISLAM M.R., LIM K.S., TAN C.G., *Monitoring corrosion process of reinforced concrete structure using FBG strain sensor*, IEEE Transactions on Instrumentation and Measurement **66**(8), 2017, pp. 2148–2155, DOI: 10.1109/TIM.2017.2676218.

[24] COOPER K.R., ELSTER J., JONES M., KELLY R.G., *Optical fiber-based corrosion sensor systems for health monitoring of aging aircraft*, [In] *2001 IEEE Autotestcon Proceedings. IEEE Systems Readiness Technology Conference. (Cat. No. 01CH37237)*, 2001, pp. 847–856, DOI: 10.1109/AUTEST.2001.949466.

[25] DONG S., LIAO Y., TIAN Q., *Sensing of corrosion on aluminum surfaces by use of metallic optical fiber*, Applied Optics **44**(30), 2005, pp. 6334–6337, DOI: 10.1364/AO.44.006334.

[26] Dong S., Peng G., Luo Y., *Preparation techniques of metal clad fibres for corrosion monitoring of steel materials*, Smart Materials and Structures **16**(3), 2007, pp. 733–738, DOI: 10.1088/0964-1726/16/3/021.

[27] McAdam G., Newman P.J., McKenzie I., Davis C., Hinton B.R.W., *Fiber optic sensors for detection of corrosion within aircraft*, Structural Health Monitoring **4**(1), 2005, pp. 47–56, DOI: 10.1177/1475921705049745.

[28] Yang D., Du L., Xu Z., Jiang Y., Xu J., Wang M., Bai Y., Wang H., *Magnetic field sensing based on tilted fiber Bragg grating coated with nanoparticle magnetic fluid*, Applied Physics Letters **104**(6), 2014, 061903, DOI: 10.1063/1.4864649.

[29] Guo T., Ivanov A., Chen C., Albert J., *Temperature-independent tilted fiber grating vibration sensor based on cladding-core recoupling*, Optics Letters **33**(9), 2008, pp. 1004–1006, DOI: 10.1364/OL.33.001004.

[30] Shen C., Zhang Y., Zhou W., Albert J., *Au-coated tilted fiber Bragg grating twist sensor based on surface plasmon resonance*, Applied Physics Letters **104**(7), 2014, 071106, DOI: 10.1063/1.4865932.

[31] Chen C., Caucheteur C., Mégret P., Albert J., *The sensitivity characteristics of tilted fibre Bragg grating sensors with different cladding thicknesses*, Measurement Science and Technology **18**(10), 2007, pp. 3117–3122, DOI: 10.1088/0957-0233/18/10/S11.

[32] Melo L.B., Rodrigues J.M.M., Farinha A.S.F., Marques C.A., Bilro L., Alberto N., Tomè J.P.C., Nogueira R.N., *Concentration sensor based on a tilted fiber Bragg grating for anions monitoring*, Optical Fiber Technology **20**(4), 2014, pp. 422–427, DOI: 10.1016/j.yofte.2014.05.002.

[33] Erdogan T., Sipe J.E., *Tilted fiber phase gratings*, Journal of the Optical Society of America A **13**(2), 1996, pp. 296–313, DOI: 10.1364/JOSAA.13.000296.

[34] Caucheteur C., Bette S., Chen C., Wuilpart M., Megret P., Albert J., *Tilted fiber Bragg grating refractometer using polarization-dependent loss measurement*, IEEE Photonics Technology Letters **20**(24), 2008, pp. 2153–2155, DOI: 10.1109/LPT.2008.2007745.

[35] Jiang B., Hao Z., Feng D., Zhou K., Zhang L., Zhao J., *Hybrid grating in reduced-diameter fiber for temperature-calibrated high-sensitivity refractive index sensing*, Applied Sciences **9**(9), 2019, 1923, DOI: 10.3390/app9091923.

[36] Li T., Dong X., Chan C.C., Zhao C.L., Jin S., *Power-referenced optical fiber refractometer based on a hybrid fiber grating*, IEEE Photonics Technology Letters **23**(22), 2011, pp. 1706–1708, DOI: 10.1109/LPT.2011.2167607.

[37] Maguis S., Laffont G., Ferdinand P., Carbonnier B., Kham K., Mekhalif T., Millot M.C., *Bio-functionalized tilted Fiber Bragg Gratings for label-free immunosensing*, Optics Express **16**(23), 2008, pp. 19049–19062, DOI: 10.1364/OE.16.019049.

[38] Ijsseling F.P., *Application of electrochemical methods of corrosion rate determination to systems involving corrosion product layers: Part 1: Linear polarization resistance measurement as an example of a simple method that can be performed with commercially available instruments*, British Corrosion Journal **21**(2), 1986, pp. 95–101, DOI: 10.1179/000705986798272316.

[39] Islam M.R., Bagherifaez M., Ali M.M., Chai H.K., Lim K.S., Ahmad H., *Tilted fiber Bragg grating sensors for reinforcement corrosion measurement in marine concrete structure*, IEEE Transactions on Instrumentation and Measurement **64**(12), 2015, pp. 3510–3516, DOI: 10.1109/TIM.2015.2459511.

Received July 15, 2021
in revised form August 22, 2021